

****TITLE****

*ASP Conference Series, Vol. **VOLUME**, **PUBLICATION YEAR***

****EDITORS****

The GMOS integral field unit: first integral field spectroscopy with an 8m telescope

Jeremy Allington-Smith¹, Graham Murray, Robert Content, George Dodsworth, Roger Davies

*Astronomical Instrumentation Group, University of Durham,
South Rd, Durham DH1 3LE, UK*

Bryan W. Miller, James Turner

Gemini Observatory, La Serena, Chile

Inger Jorgensen

Gemini Observatory, Hilo, Hawaii, USA

Isobel Hook²

UK Gemini Project Office, University of Oxford, Oxford, UK

David Crampton, Richard Murowinski

Herzberg Institute of Astrophysics, Victoria, BC, Canada

Abstract.

The Gemini Multiobject Spectrograph (GMOS) installed on the Gemini-North telescope has a facility for integral field spectroscopy over the wavelength range 0.4–1.0 μ m. GMOS is converted to this mode by the remote insertion of an integral field unit (IFU) into the beam in place of the masks used for multiobject spectroscopy. With the IFU deployed, integral field spectroscopy is available over a fully-filled contiguous field of 5×7 arcsec with a sampling of 0.2 arcsec. A separate field of half the area, but otherwise identical, is also provided to aid background subtraction. The IFU contains 1500 lenslet-coupled fibres and is the largest-format fibre-based IFU yet tested on the sky and the first facility of any type for integral field spectroscopy employed on an 8/10m telescope. We describe the IFU and present results from commissioning.

¹e-mail: j.r.allington-smith@durham.ac.uk

²address: Gemini North Observatory

1. Introduction

The first of the two Gemini Multiobject Spectrographs has been completed and tested on the Gemini-North Telescope. This paper describes the integral field unit (IFU) which converts this multiobject spectrograph into an integral field spectrograph.

The capabilities of GMOS (Fig. 1) can be summarised as follows.

- 0.07 arcsec/pixel image scale
- 5.5×5.5 arcmin field
- 0.4 - $1.1\mu\text{m}$ wavelength coverage
- Resolving power up to $R = 10,000$ (with 0.25 arcsec slits)
- Detector: CCD mosaic of $3 \times (4608 \times 2048)$ pixels
- Active control of flexure
- On-instrument WFS for accurate guiding
- Main modes:
 - Multiobject using laser-cut slit masks
 - Integral field spectroscopy mode
 - Longslit spectroscopy using generic masks
 - Imaging

The scientific requirements were defined by the Gemini project. These are summarised below, where the adopted top-level specification and main design features are also given.

- To exploit good images from GEMINI, the IFU has a sampling of 0.2 arcsec.
- To provide unit filling factor in the field, the fibres are coupled to a close-packed lenslet array at the input
- To provide the largest possible contiguous field, 1000 fibres were used to give an object field of 7×5 arcsec (1000 fibres)
- To make provision for accurate background subtraction, an extra 5×3.5 arcsec field offset by 60 arcsec from the object field is provided for background estimation (500 fibres).
- To allow a transparent change between slit and integral field modes, the IFU is deployed by the mask exchanger and the input and output foci are coplanar with the masks.
- To obtain high throughput, the fibres are lenslet-coupled at the output and input to convert the F/16 beam to $\sim\text{F}/5$ for efficient use with fibres.

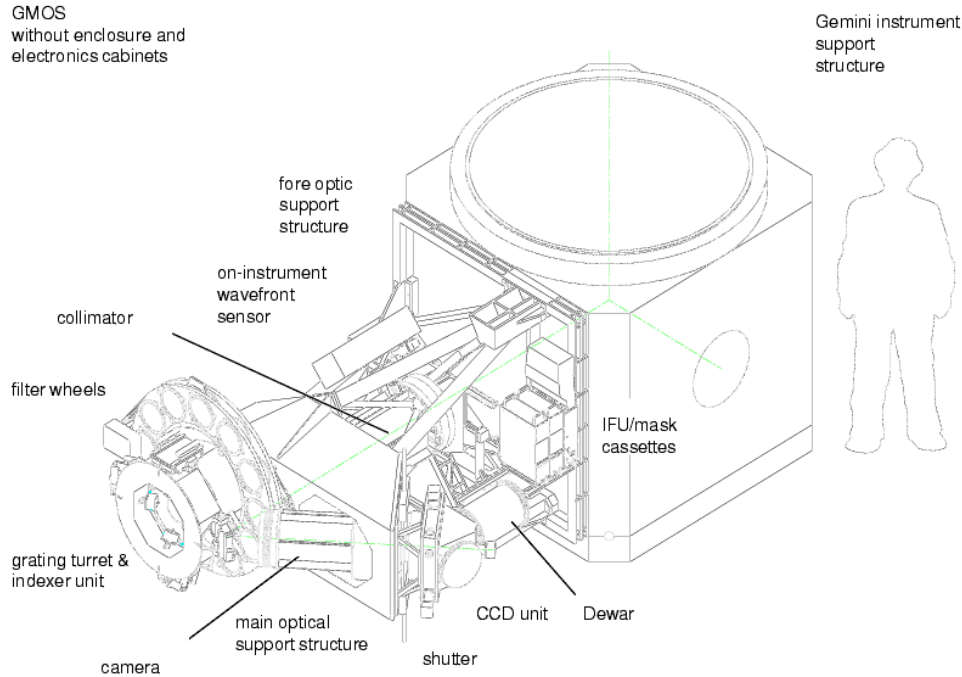


Figure 1. Mechanical layout of GMOS without its enclosure and electronics cabinets mounted on the instrument support structure (ISS) of the Cassegrain focus. It is shown in a sideways-looking mounting but may be mounted in an upward-looking orientation by attaching it to the lower face of the ISS.

- The adoption of a low risk construction technique (to reduce risk to schedule) dictated the use of the fibre+lenslet technique in preference to image slicing (see Allington-Smith & Content 1999 — hereafter AC — for a summary of the techniques available)

2. Description

The principle of the optical design is shown in Fig. 2. We used the fibre-lenslet technique described by AC. This makes more efficient use of the detector surface than the lenslet-only approach (e.g. Sauron; Bacon et al 2001). While not quite as efficient as the image-slicing method (e.g. 3D; Weitzel et al. 1996), it provides a high level of efficiency without the technical risk that would be required to implement such a design. The original image-slicing technique of 3D could not be used for reasons of size and optical performance, but a version using the *Advanced Image Slicer* (AIS) concept would have been feasible for GMOS (Content 1997). Although IFUs using the AIS concept are under construction

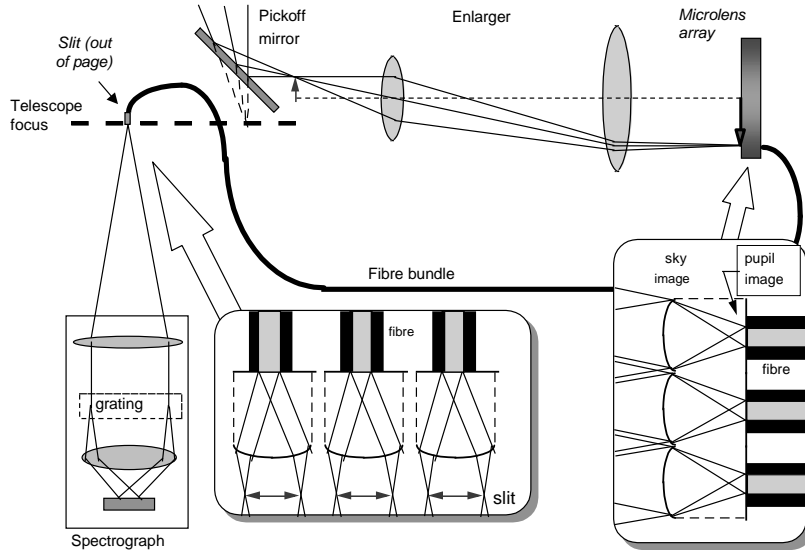


Figure 2. Principle of the GMOS-IFU. The insets show details of the fibre-lenslet coupling at the input and output of the IFU.

(Dubbeldam et al. 2000), the technology, employing diamond-turned spherical optics, was deemed to pose an unacceptable risk to GMOS's tight schedule.

The design adopted folds light approaching the telescope focal plane into a telecentric enlarger which re-images the field onto a close-packed lenslet array. This produces an array of pupil images which are fed into optical fibres in a fast beam to minimise the effect of focal ratio degradation (FRD; Carrasco & Parry 1994). This arrangement ensures that the filling factor in the field is nearly unity since it is set by the the lenslet array, which is close-packed, rather than by the fibres whose active area, that of the cores, is sparsely distributed.

The fibres allow the 2-D array to be reformatted into two pseudo-slits which are located at the original telescope focal plane. By splitting the fibres into blocks which may be individually aligned, it is possible to mimic the exit pupil of the telescope so that the spectrograph receives the reformatted light as if from a pair of conventional longslits. These slit blocks contain the fibre terminations which consist of linear lenslet arrays which convert the beam back to the speed originally incident from the telescope.

The confocality of the input and output focal surfaces of the IFU with that of the telescope means that no major shift in spectrograph focus is required when the IFU is inserted into the beam. Thus, the deployment of the IFU is a transparent process from the point of view of the spectrograph.

In the normal two-slit mode, two sets of spectra are produced, displaced in the dispersion direction. This allows the spectra to contain ~ 2000 pixels but

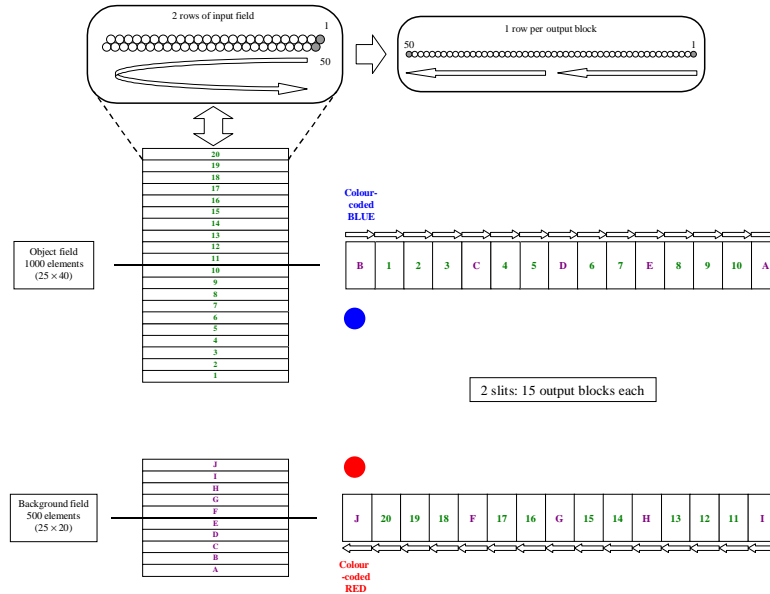


Figure 3. The mapping between field and slit. The two fields are shown schematically on the left and the two slits on the right. The division of each field into blocks (each containing 2 rows at the input) is shown. The arrows indicate how the elements in a row map onto the slit. Each slit maps to one contiguous half of each field, so that the IFU can be used with one slit only to maximise spectrum length at the expense of field area.

requires the use of a suitable bandpass filter to avoid overlaps between spectra. If it is desired to increase the spectrum length and avoid the possibility of overlaps altogether, one slit may be blocked off by the manual insertion of an output mask. The mapping between the field and the slit is arranged so that this will block off one half of both object and background field leaving contiguous sections of the field as shown in Fig. 3. This allows the observer to choose the optimum combination of the numbers of spectral and spatial samples.

In order to maximise the numbers of spatial samples, the images produced by each fibre at the pseudoslit are allowed to overlap slightly. This situation is discussed by AC, who show that the only consequence is a slight degradation in spatial resolution (in the direction corresponding to that of the slit only) since the Nyquist sampling criterion is satisfied providing that the object is sampled by at least two lenslets at the IFU input: the sampling of the slit by the detector is only of minor importance. If the overlap between images at the slit was minimised, the result would be a drastic reduction in the number of spatial samples with a consequent reduction of the field of view. The close-packed configuration also requires that the mapping between the input and output is such that elements which are adjacent at the slit are also adjacent in the field, as shown in Fig. 3,

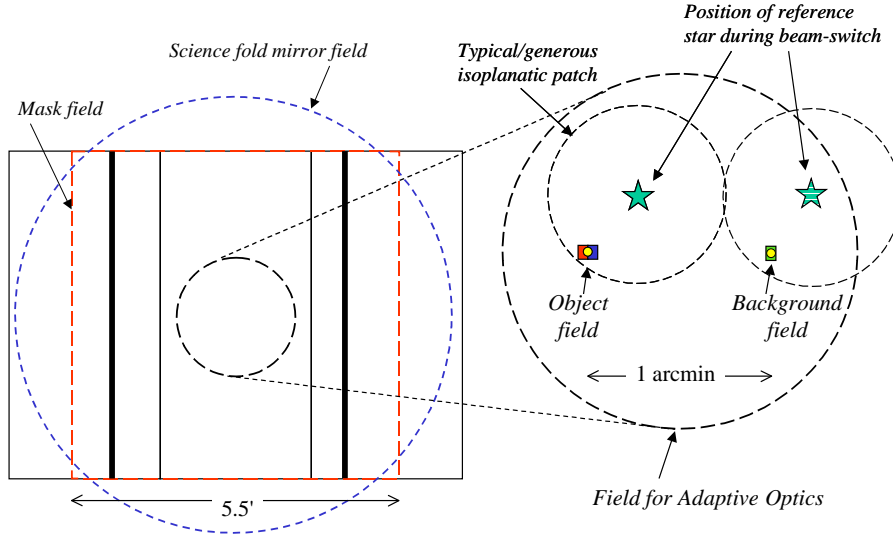


Figure 4. Layout of the main GMOS and IFU fields. On the left the field of view of GMOS is given by the intersection of the circular field of the science fold mirror and the square field covered by the slit mask (both dashed). This is shown projected onto the detector, a mosaic of three CCDs, indicated by the thin solid lines. The thick lines show the location of the IFU slits. The central portion of the GMOS field is enlarged (right) to show the location of the two IFU fields and the typical disposition of a reference star for both segments of a typical beam-switch cycle, shown as stars. The field of the AO system and a typical isoplanatic patch is also indicated.

and that the element-to-element variation in throughput is small, as described in Section 3.2.

The quality of background subtraction can be enhanced by the use of the separate background field. This is half the size of the object field and separated from it by 60 arcsec to allow the centre of a large extended object to be observed while still obtaining a clean estimate of the sky background (Fig. 4). If desired, beam-switching may be used, by which the telescope is nodded to switch the object alternately between the object and background field. This provides immunity to temporal variations in the sky background, depending on the frequency of switching, and improves the subtraction accuracy since the same physical elements sample both object and sky. This is discussed in detail by AC.

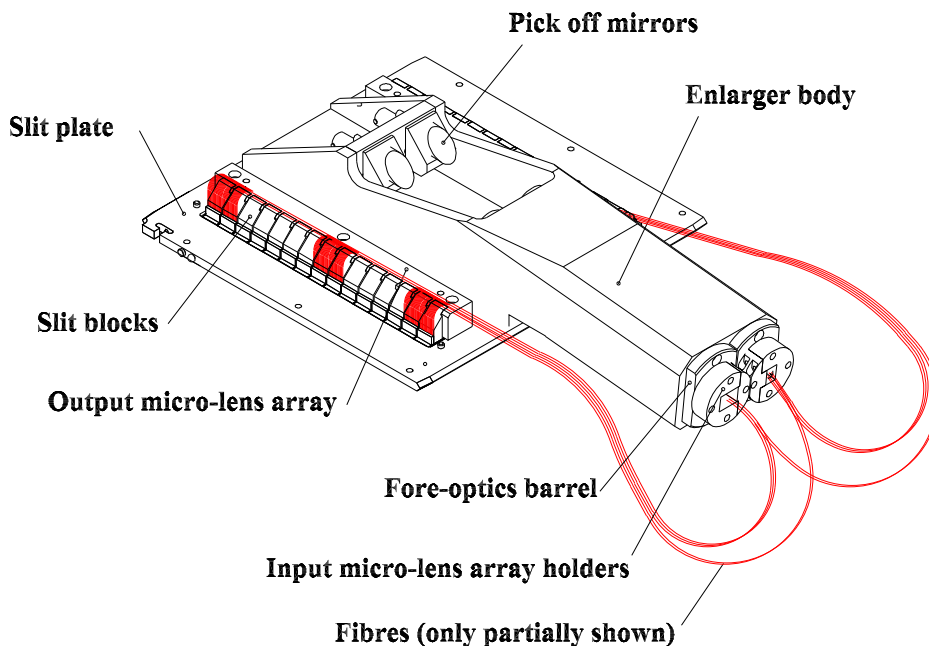


Figure 5. Three-dimensional drawing of the IFU without covers.

Fig. 5 gives an overview of the mechanical design. The fore-optics and slit assemblies are fixed rigidly to the slit plate. The slit plate interfaces with the mask exchange mechanism in the same way as for a regular slit mask.

3. Instrument characterisation

The performance of the IFU was determined by measurements in the laboratory after assembly and at the telescope, in September 2001, during the commissioning of GMOS.

3.1. Cosmetic quality

Out of 1500, there is only one broken element. In addition there are 4 elements with significantly reduced throughput (assessed by visual inspection).

3.2. Throughput and fibre-to-fibre variation

The throughput of the IFU was measured in the laboratory using a calibrated photodiode referenced to a wavelength of 670nm.

The throughput of the complete IFU without regard to the spectrograph stop (i.e. without constraining the angular extent of the output beam) was found to be $79\pm 5\%$. The useful component of this throughput (i.e. all light that enters the spectrograph stop) was determined to be $68\pm 5\%$. This figure includes any slit-pointing misalignment. This compares with the theoretical estimate made before final system optimisation of 59%.

The throughput of the IFU after installation on the telescope was assessed using flatfield light from the Gemini Calibration Unit (GCAL). The IFU was deployed in GMOS and an exposure made in direct imaging mode (the grating replaced by a plane mirror) with a particular broad-band filter in the beam. The resulting raw data was examined and the signal integrated over the full extent of the IFU output (the direct images of the two slits) after subtracting the detector background. The IFU was then removed from the beam and another direct image taken with the same spectrograph and GCAL configuration. The signal was summed over those pixels which correspond to the spatial extent of the two input fields of the IFU. A comparison of the signal levels yields the throughput of the IFU alone over the passband defined by the filter. The results were: 62%, 65%, 62% and 58% in the g' , r' , i' and z' filter passbands respectively (SDSS system: Fukugita et al. 1996). The previous laboratory measurement of $68 \pm 5\%$ (670nm) is consistent with the r' -band result (550-700nm).

This is the simplest and most direct method of measurement because it is independent of variations in seeing or transparency that might affect an observation of a standard star.

The variation in throughput from fibre to fibre was estimated from flat-field data. Ignoring the 5 elements known to be defective, the counts recorded in each extracted spectrum showed an RMS variation of 6%. This is an upper limit since the intensity of the flatfield illumination was not completely uniform.

3.3. Image quality

The same commissioning data were used to assess the quality of the images of the individual elements at the slit, as recorded by the detector. In direct imaging mode, these appear as a series of round images aligned in the spatial direction. Each is clearly resolved and the images overlap at $\sim 50\%$ of their peak value in the spatial direction. Fig. 6 shows a close-up of one slit block and a cut in the spatial direction which also shows the extent of the inter-block gap.

3.4. Stability

Flexure effects were assessed by recording the positions of the images of the IFU slit as a function of gravity vector while the telescope is placed in different orientations. Although some flexure is seen (typically 0.1 pixel/hour), it is similar to that experienced by GMOS without the IFU deployed (in direct-image or slit-spectroscopic modes). Thus we conclude that any contribution from the movement of the IFU as a whole or from its component parts is too small to be measurable. The precision of this result is limited by non-repeatability in the measurements. This is made up of a combination of some intrinsic non-elasticity in the structure of GMOS and the uncertainty in measuring the centroids of the images.

4. Scientific characterisation

During commissioning, a number of elliptical galaxies from the Sauron programme (de Zeeuw et al. 2002) were observed in order to provide a comparison dataset to allow us to verify the accuracy of the data reduction. In addition,

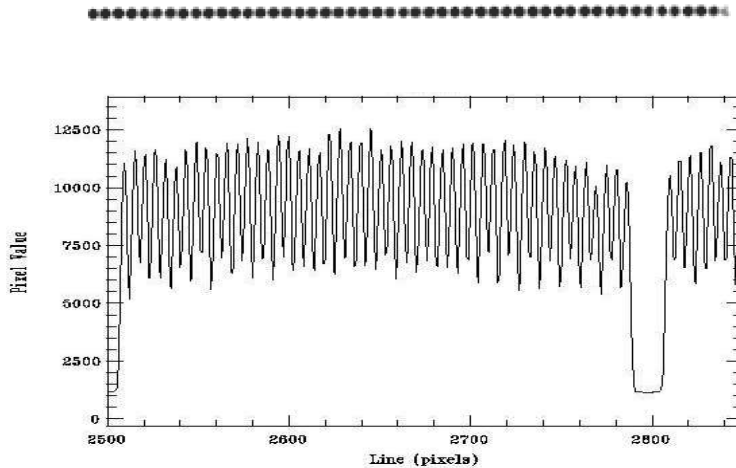


Figure 6. Top: an image of a slit block obtained with GMOS in direct-imaging mode showing the individually resolved images of each element. The dispersion direction is vertical. Bottom: a cut in the spatial direction (not to scale) also showing an inter-block gap.

NGC 1068 was observed to allow a comparison with the extensive body of long-slit spectroscopy available with e.g. STIS on the Hubble Space Telescope (Crenshaw & Kraemer 2000) as well as previous integral field data, (e.g. Thatte et al. 1997, Pecontal et al. 1997, Garcia-Lorenzo et al. 1999).

The observations of NGC1068 consist of a set of 4 pointings offset from the object centre by a few arcsec so as to synthesise a larger field by mosaicing. We used the B600 grating with the g' filter to limit the length of spectrum so as to avoid overlap between the two sets of spectra. This configuration gave good coverage of the $H\beta$ and $[OIII]4959+5007$ emission lines.

Fig. 7 shows a comparison of a direct image of NGC 1068 taken by GMOS with the g' filter and an image in the same passband reconstructed from the integral field data. They are very similar, with only small differences that are likely to be caused by the small difference between the passband of the direct image and that used in the reduction of the spectroscopic data. This provides a preliminary check of the accuracy of the integral field data.

Fig. 8 shows how the shape and multiplicity of the emission lines changes over the field. This confirms the initial impression of complexity obtained from examination of the raw data.

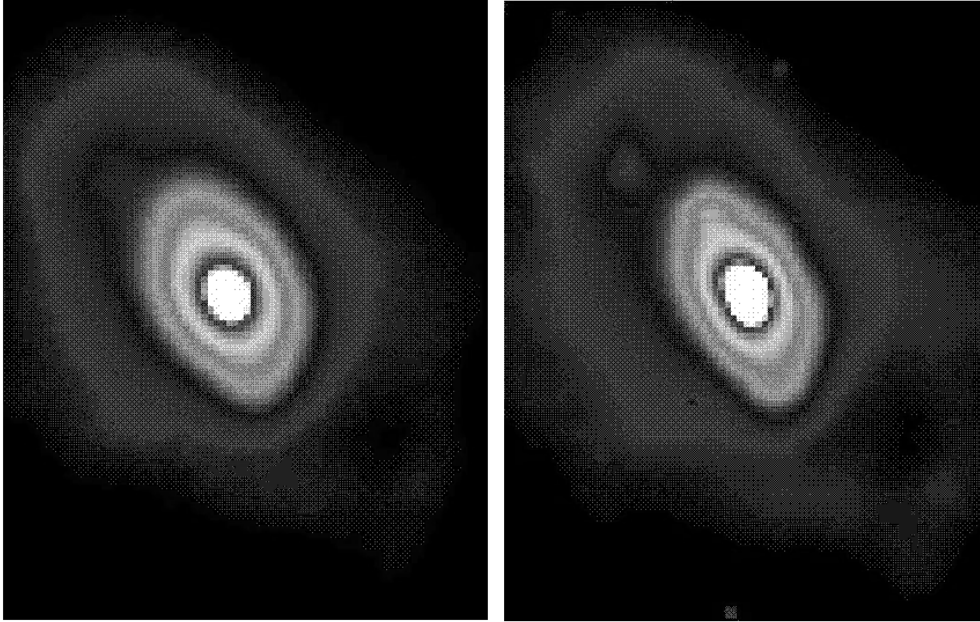


Figure 7. A comparison of a direct image of the nuclear region of NGC1068 taken with GMOS in imaging mode (left) and reconstructed from the integral field data (right) using the same g' passband filter (although the passband used for spectrum extraction does not cover the full filter passband). The IFU data is a mosaic of four pointings. Both images are resampled to 0.1 arcsec/pixel. The field shown is 10 arcsec in width. North is up and East is left.

These data were reduced using a software package produced by GEMINI for GMOS. This includes special features for the reduction of integral field data, which is generally more complex than for slit spectroscopy.

5. Conclusions

We have described the design of the integral field unit of the Gemini Multiobject Spectrograph installed on the northern Gemini telescope and presented performance results obtained in the laboratory and at the telescope. This is the first instrument for integral field spectroscopy on an 8-10m telescope and the largest format of fibre-coupled IFU yet used at any telescope.

Estimates of the throughput of the IFU (including losses at the spectrograph stop) indicate reasonable agreement between theory and measurements in the laboratory, considering that both determinations are subject to uncertainties which are difficult to estimate. The experimentally-determined throughput is a little higher than expected indicating the high quality of construction and the realism of the theoretical model, which made pessimistic assumptions where hard data was lacking. This encourages us to believe that not only have we developed the techniques to make high-quality devices for integral field spectroscopy but

also that we have the design tools which allows us to make a near-optimal choice of design parameters and produce realistic estimates of the final performance.

Measurements obtained at the telescope indicate a throughput intermediate between the laboratory and theoretical estimates, although formally consistent with the former. The variation in throughput between elements is satisfactorily small and the quality of the images at the slit is actually slightly better than predicted. This is expected to ease the task of data reduction.

Acknowledgments. We thank the many staff in Durham who have worked on the GMOS-IFU or on its prototypes: Roger Haynes, David Lee, Ian Lewis, Deqing Ren, Jingyun Zhang, Ray Sharples and David Robertson. We also thank the other members of the GMOS team who made this work possible by supplying the superb optics, mechanics, electronics and controls of GMOS-1, including Terry Purkins, Phil Williams and David Lunney. We also thank the Gemini project for supporting this work (especially Doug Simons, Fred Gillett and Matt Mountain).

The Gemini Observatory is operated by the Association of Universities for Research in Astronomy, Inc., under a cooperative agreement with the NSF on behalf of the Gemini partnership: the National Science Foundation (United States), the Particle Physics and Astronomy Research Council (United Kingdom), the National Research Council (Canada), CONICYT (Chile), the Australian Research Council (Australia), CNPq (Brazil) and CONICET (Argentina).

References

- Allington-Smith, J. & Content, R., 1999. *PASP* 110, 1216-1234.
- Bacon, R., Copin, Y., Monnet, G., Miller, B.M., Allington-Smith, J.R., Bureau, M., Carollo, C.M., Davies, R.L., Emsellem, E., Kuntschner, H., Peletier, R.F., Verolme, E.K. & de Zeeuw, T., 2001. *MNRAS* 326, 23.
- Carrasco, E. & Parry, I., 1994. *Mon. Not. R. Astron. Soc.*, 271, 1
- Content, 1997. *SPIE* 2871, 1295-1305
- Crenshaw, D. & Kraemer, S., 2000. *ApJ*, 532, L101-L104.
- Dubbeldam, M., Content, R., Allington-Smith, J., Pokrovsky, S., Robertson, D., 2000. *SPIE* 4008, 1181-1192.
- Fukugita, M., Ichikawa, T., Gunn, J. E., Doi, M., Shimasaku, K., & Schneider, D. P. 1996. *A.J.* 111, 1748.
- Garcia-Lorenzo, B., Mediavilla, E. & Arribas, S., 1999. *ApJ* 518, 190-212.
- Pecontal, E., Ferruit, P., Binette, L. & Wilson, A.S., 1997. *ApSS* 248, 167-174.
- Thatte, N., Genzel, N., Kroker, H., Krabbe, A., Tacconi-Garman, L., Maiolino, R. & Tecza, M., 1997. *ApSS* 248, 225-234.
- Weitzel, L., Krabbe, A., Kroker, H., Thatte, N., Tacconi-Garman, L. E., Cameron, M., and Genzel, R. 1996. *Astr. & Astroph. Suppl.*, 119, p 531.
- de Zeeuw, P. T, Bureau, M., Emsellem, E, Bacon, R., Carollo, C.M., Copin, Y., Davies, R. L., Kuntschner, H, Miller, B.W, Monnet, G., Peletier, R. F. & Verolme, E. K., 2002. *MNRAS* 329, 513.

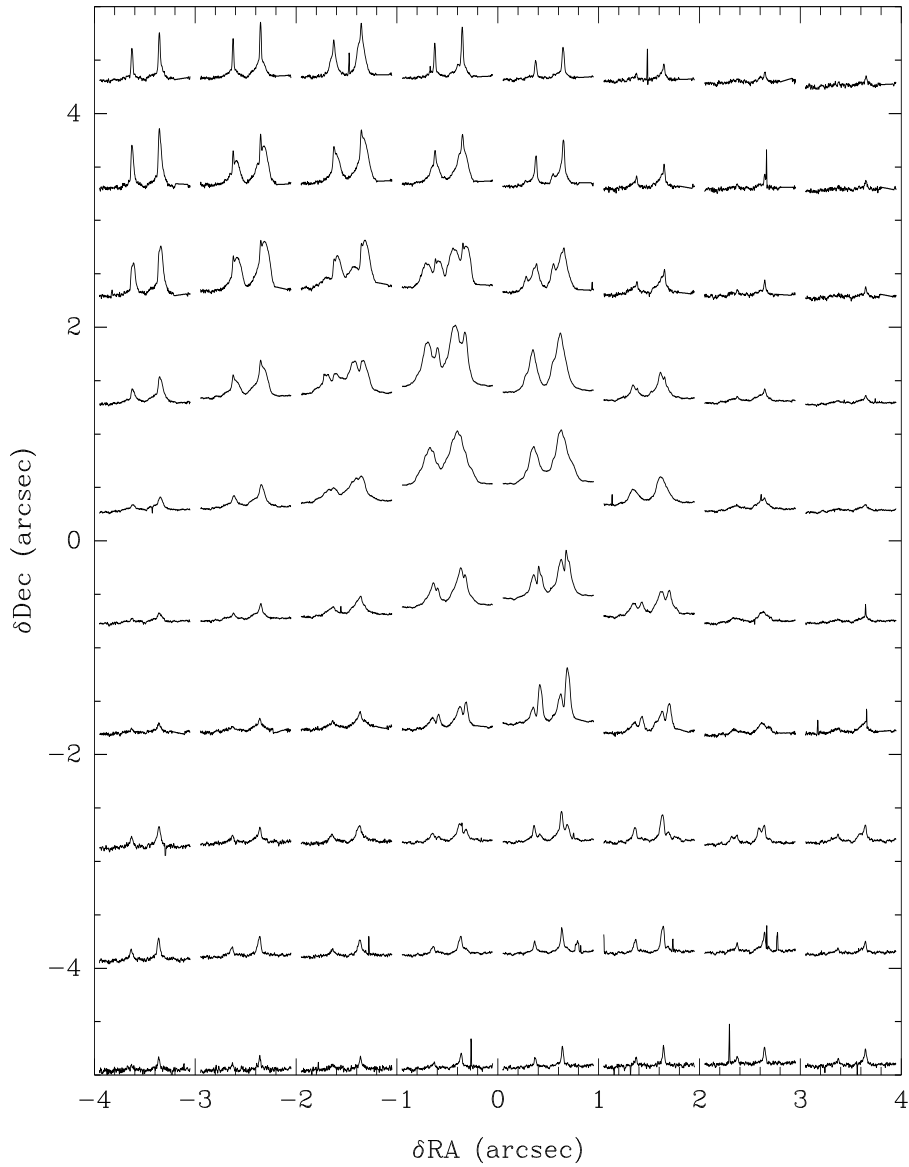


Figure 8. A composite plot of the [OIII]4959+5007 emission lines over the field. The shape of the lines varies strongly and multiple components are evident.